Lattice preamorphization by ion irradiation: Fluence dependence of the electronic stopping power threshold for amorphization

F. Agulló-López, G. García, and J. Olivares

Citation: J. Appl. Phys. **97**, 093514 (2005); doi: 10.1063/1.1896444
View online: http://dx.doi.org/10.1063/1.1896444
View Table of Contents: http://jap.aip.org/resource/1/JAPIAU/v97/i9
Published by the American Institute of Physics.

Lattice preamorphization by ion irradiation: Fluence dependence of the electronic stopping power threshold for amorphization

F. Agulló-López[a)]
Departamento de Física de Materiales, C-IV, Universidad Autónoma de Madrid, Cantoblanco, E-28049 Madrid, Spain and Centro de Microanálisis de Materiales (CMAM), Universidad Autónoma de Madrid, Cantoblanco, E-28049 Madrid, Spain

G. García
Centro de Microanálisis de Materiales (CMAM), Universidad Autónoma de Madrid, Cantoblanco, E-28049 Madrid, Spain

J. Olivares
Instituto de Óptica "Daza de Valdés", Consejo Superior de Investigaciones Cientificas (CSIC), Calle Serrano 121, E-28006 Madrid, Spain

(Received 4 November 2004; accepted 28 February 2005; published online 20 April 2005)

A thermal-spike model has been applied to characterize the damage structure of the latent tracks generated by high-energy ion irradiations on $LiNbO_3$ through electron excitation mechanisms. It applies to ions having electronic stopping powers both below and above the threshold value for lattice amorphization. The model allows to estimate the defect concentrations in the heavily damaged (*preamorphized*) regions that have not reached the threshold for amorphization. They include the *halo* and *tail* surrounding the *core* of a latent track. The existence of the preamorphized regions accounts for a synergy between successive irradiations and predicts a dependence of the amorphization threshold on previous irradiation fluence. The predicted dependence is in accordance with irradiation experiments using N (4.53 MeV), O (5.00 MeV), F (5.13 MeV), and Si (5 and 7.5 MeV). For electronic stopping powers above the threshold value the model describes the generation of homogeneous amorphous layers and predicts the propagation of the amorphization front with fluence. A theoretical expression, describing this propagation, has been obtained that is in reasonable agreement with silicon irradiation experiments at 5 and 7.5 MeV. The accordance is improved by including in a simple phenomenological way the *velocity effect* on the threshold. At the highest fluences (or depths) a significant discrepancy appears that may be attributed to the contribution of the nuclear collision damage. © *2005 American Institute of Physics*.
[DOI: 10.1063/1.1896444]

I. INTRODUCTION

High-energy ion bombardment of materials is a well-known method for material modification.[1–4] This includes ion implantation that is routinely used in the semiconductor industry for impurity doping. During the trajectory of the bombarding ion in the target material two mechanisms account for energy losses. At high energy electronic excitation losses are dominant whereas at lower energies elastic nuclear collisions are mainly responsible for the slowing down of the ions. The nuclear damage mechanism is well-documented and proceeds via displacement cascades. It becomes most effective for the low ion energies occurring at the end of the track. For high-enough fluences the lattice becomes heavily damaged and finally amorphized. This amorphization has often been used in the case of transparent insulator materials for the fabrication of optical waveguides and integrated optics devices.[4]

In many analysis the generation of stable lattice damage as a consequence of electronic excitation is ignored. However, it is known for a long time that the electronic excitation mechanism may lead to permanent damage along the ion track if a certain threshold in the electronic stopping power is reached or surpassed.[5–8] In this case, an amorphous linear region, known as a latent track, is formed along the ion trajectory. These latent tracks can be chemically etched and they provide a sensitive method for ion (particularly fission fragments) detection and counting in dosimetry and dating applications.[7] More recently a large number of micro- and nanosystems, that use etched or etched and filled tracks, are being proposed or tested. They include a variety of photonic and magnetic media.[9–14]

Most theoretical models dealing with the formation of the latent track use the concept of thermal spike.[15–24] The deposited electronic excitation energy density S_e during the passage of the ion is rapidly transferred to the ion lattice. It causes a sudden increase of the temperature and eventually the local melting of the crystal. Subsequent fast quenching of the structure turns the melt into an amorphous state. Different mathematical approaches have been considered. In particular, the detailed model put forward by Toulemonde *et al.*,[17,18] describes the electron–electron and electron–phonon interactions by a set of differential equations and predicts track diameters in accordance with experiments after a suit-

[a)]Author to whom correspondence should be addressed; electronic mail: fal@uam.es

able choice of the electron mean free path.[20,24] Similar thermal-spike models have been applied to describe other effects related to strong electron excitation such as ion sputtering,[25,26] laser damage,[25] and swelling.[27] Although powerful molecular-dynamics[26,28,29] and hydrodynamics[30] methods have been developed to tackle these complex problems, they require extensive numerical calculations and are not free of some critical assumptions. Moreover, they have been, so far, applied to simple solids containing a single atomic species. Therefore, thermal-spike models are still needed since they offer simple analytical expressions that may reasonably describe many experimental features and trends.

The purpose of this paper is to extend the thermal-spike model[16,24] to discuss preamorphization stages in $LiNbO_3$, i.e., the generation of preamorphized regions during ion irradiation. As far as we know this problem has not been investigated and we consider that thermal-spike models provide a suitable framework to deal with these stages and the transition to a fully amorphous crystal. It is appropriate to state here that it is not essential for the model to assume a thermal equilibrium distribution of atom velocities. The key point is to assume that the distribution can be adequately characterized by an average value or an effective temperature. Previous experimental data[31–33] and particularly those described in this paper show that a homogeneous amorphous layer with a sharp boundary is generated under irradiation for fluences above a critical value. Moreover, a threshold in the electronic stopping power appears to be required to initiate amorphization. All these data suggest that the formation of the amorphous layer is caused by electronic excitation mechanisms and, therefore, related to the generation of individual latent tracks. When a critical fluence corresponding to overlapping of such tracks is achieved, the layer is formed. On the other hand, it is shown in this paper that the thickness of the amorphous layer increases with fluence, i.e., the inner boundary of the layer moves into the crystal. We consider that the preamorphization concept appears useful or even necessary to account for all these relevant results.

Section II presents the essentials of the thermal-spike model as applied to the preamorphization stages. Section III describes the morphology of the preamorphized regions around a single latent track. Section IV A summarizes the main experimental results showing the synergy between successive irradiations. Sections IV B and IV C present in detail the model to account for the memory effect, i.e., the dependence of threshold on previous irradiation fluence and the propagation of the amorphization boundary. Comparison of the theoretical predictions to the experimental results is discussed in Sec. IV A. Finally, Sec. V offers a summary of the results and some final conclusions. It is expected that the model will contribute to stimulate further theoretical and experimental work on these topics.

II. THEORETICAL MODEL

The proposed theoretical model is based on the thermal-spike approach by Szenes.[16,19] It has the advantage of not requiring a detailed formulation of the electron and ion dynamics after irradiation accounting for the heat transport processes. Moreover, it can be easily extended to take into account preamorphization stages. The model is summarized here. The ion transfers an energy S_e per unit length to the electron system. This energy is then passed onto the ionic lattice with a certain efficiency factor $g<1$ independent of S_e. The transferred energy generates a certain temperature distribution $\Delta T=\Delta T(r,t,S_e)$. At $t=0$ we assume a Gaussian distribution:

$$\Delta T(r,0,S_e)=\frac{Q}{2\pi a_0^2\rho C}e^{-r^2/2a_0^2}, \tag{1}$$

where a_0 is the width of the initial Gaussian distribution, ρ the crystal density, and C the specific heat. $\Delta T=T-T_s$, T_s being the substrate temperature and $Q=gS_e$ the energy per unit length transferred to the ionic lattice. To describe the evolution of the temperature profile with time the model uses some assumptions that are, here, explicitly summarized:

(a) The area under the Gaussian is preserved. This condition requires that heat conduction is the only heat transport mechanism, i.e., radiation is neglected.
(b) The mechanical and thermal parameters do not depend on temperature, which is a reasonable assumption at high temperatures (near the melting point).
(c) The heat conduction in the direction perpendicular to the input surface is ignored so that at every depth the transport processes are two dimensional.

From these assumptions $\Delta T(r,t,S_e)$ can be obtained for $t>0$ arbitrarily. The maximum temperature obtained for any $t>0$ at a given distance r from the impact point is then[16]

$$\Delta T_{\max}(r,S_e)=\frac{gS_e}{2\pi a_0^2\rho C}e^{-r^2/2a_0^2}, \quad 0<r<\sqrt{2}a_0, \tag{2a}$$

$$\Delta T_{\max}(r,S_e)=\frac{gS_e}{\pi e\rho C}\frac{1}{r^2}, \quad r>\sqrt{2}a_0. \tag{2b}$$

Notice that the maximum of those temperatures is attained at $r=0$:

$$\Delta T_{\max}(0,S_e)=\frac{gS_e}{2\pi a_0^2\rho C}. \tag{3}$$

In particular, taking $\Delta T_{\max}=\Delta T_m=T_m-T_s$, T_m being the melting temperature of the crystal, the critical required stopping power S_m is obtained through

$$\Delta T_m=\frac{gS_m}{2\pi a_0^2\rho C}. \tag{4}$$

One can then calculate the radius of the region that has reached a temperature $T_{\max}$ above a given value of T. Particularly, selecting $T_{\max}>T_m$ one defines the *core* of the track. The core radius R_c is thus

$$R_c^2=r^2(T_m)=2a_0^2\log\frac{S_e}{S_m}, \quad 0\leqslant R_c^2\leqslant 2a_0^2, \tag{5a}$$

$$R_c^2 = r^2(T_m) = \frac{2a_0^2}{e}\frac{S_e}{S_m}, \quad R_c^2 \geqslant 2a_0^2. \tag{5b}$$

At any depth z the radius of the core is determined by the electronic stopping power curve $S_e(z)$. Equations (3)–(5) are the basis of the analysis that follows.

The key proposal of our model is that the defect structure of the region at and around the track is determined from the maximum temperature reached after the passage of the ion. The quenching rate is assumed to be fast enough to freeze the thermally generated defect concentration. In fact, although the melting point is not reached the concentration of intrinsic defects causing lattice disorder in the crystal may become very high and generate what can be designated as a *preamorphized* region (see Sec. III).

We will assume that the concentration of intrinsic defects generated by the swift ion and responsible for the structural damage is given[2] by some effective Arrhenius law,

$$c(T) = Ae^{-\varepsilon/kT}. \tag{6}$$

This Arrhenius dependence is well established for the defect concentration achieved in thermal equilibrium at a temperature T. Then, ε is the formation energy of the responsible defect and A a factor related to the formation entropy s of the defect, $A=e^{s/k}$. However, in our case where thermal equilibrium is not guaranteed the dependence should still apply with a different meaning for the parameter ε. In fact, Eq. (1) simply states the probability for fast atoms with average kinetic energy $3kT/2$ to overcome a certain effective energy barrier ε and cause disorder. In a way, the production of defects may follow a quite analogous path to that involved in nuclear collision damage. In expression (1) T is the maximum temperature reached in the spike caused by the bombarding ion. It is not easy to decide on the kind of defects responsible for the thermally induced disorder and eventually the melting of the crystal.[2,34] At the present stage of the model the energy barrier ε should be, essentially, considered as an adjustable parameter.

Our approach also assumes that the radiation-induced defects at the damaged (preamorphized) regions add to those generated by another irradiation, i.e., damage is cumulative. This behavior is well established for nuclear collision damage but it is less assured for electronic excitation damage. However, one may quote evidence of damage accumulation under swift-ion irradiation[35] as well as other types of electronic excitation.[36] In our experiments the irradiation-induced defects generated in the spike rearrange through some short-range processes into stable structures (distorted octahedra, dislocation loops, amorphized spots, etc.) that cause a local distortion of the lattice. It may be stable versus additional swift-ion irradiation. Anyhow, the experimental data to be described in this paper and those reported in previous publications[31,33] clearly point out to the generation of stable damage by electronic processes and also to the accumulative nature of such damage even below threshold. In spite of the uncertainties in the microscopic description of the damage, which are inherent to spike models, our theoretical analysis provides a satisfactory description of the main features and trends of the irradiation behavior in terms of ε as a key adjustable parameter.

III. TRACK STRUCTURE: CORE, HALO, AND TAIL

In order to determine the lattice structure around the ion trajectory one should define a certain critical defect concentration to initiate or nucleate the melted and subsequently amorphous phase (*core*) as well as to characterize the damaged or preamorphized regions around (*halo*) and below (*tail*) the core. In many crystals the critical melting concentration c_m, derived from a comparison to experimental data,[37] is roughly around 10^{-3} (normalized to atomic concentration). As to the so-called preamorphized regions (halo and tail), one may safely consider that they should contain a defect concentration $c_h/c_m \geqslant 10^{-3}$, i.e., c_h over 10^{-6}, which represents some typical background concentration of defects. Anyhow, the particular values assumed for these concentrations, c_m and c_h, are a matter of convention and do not enter directly in any of the predictions of the model (see below). By replacing c_h into expression (6) one obtains that the temperature reached at this boundary is

$$T_h = \frac{T_m}{1 - \dfrac{kT_m}{\varepsilon}\log_e\dfrac{c_h}{c_m}}. \tag{7}$$

Then, following the same procedure leading to (5) one obtains that the radius R_h of the halo at a depth z is

$$R_h^2(z) = r^2(T_h) = 2a_0^2 \log_e[S_e(z)/S_h]$$

$$= R_c^2 + 2a_0^2 \log_e\frac{S_m}{S_h}, \quad 0 \leqslant R_h^2 \leqslant 2a_0^2, \tag{8a}$$

$$R_h^2(z) = r^2(T_h) = \frac{2a_0^2}{e}\frac{S_e(z)}{S_h} = R_c^2\frac{S_m}{S_h}, \quad R_h^2 \geqslant 2a_0^2, \tag{8b}$$

where S_h is the electronic stopping power leading to a maximum temperature T_h. Notice that S_m/S_h can be replaced by $\Delta T_m/\Delta T_h$ [see Eq. (3)], which can in turn be obtained from Eq. (7). The core radius squared of the latent track is increased in the fixed amount $2a_0^2 \log_e(S_m/S_h)$ for values of S_e close to the threshold. For high-enough electronic stopping power where R_h^2 and R_c^2 depend linearly on S_e, the ratio of the halo and core radii squared remains constant and equal to S_m/S_h. The profiles of R_c and R_h in $LiNbO_3$ under silicon irradiation at 7.5 MeV are illustrated in Fig. 1 as a function of depth z. The halo profiles for other choices of c_h are also included for comparison. Notice that it is not necessary to assume any specific value for c_m but just c_m/c_h. For this particular example the selected parameters have been $a_0 = 5.5$ nm, $S_m = 4.75$ keV/nm, and $kT_m/\varepsilon = 0.2$ ($\varepsilon = 0.63$ eV). These values have been chosen in order to clearly illustrate the appearance of the track core. A slightly higher value of 5.2 keV/nm for S_m, obtained from direct comparison to experimental data, is used in the following sections. On the other hand, the length of the tail along the ion trajectory is given by

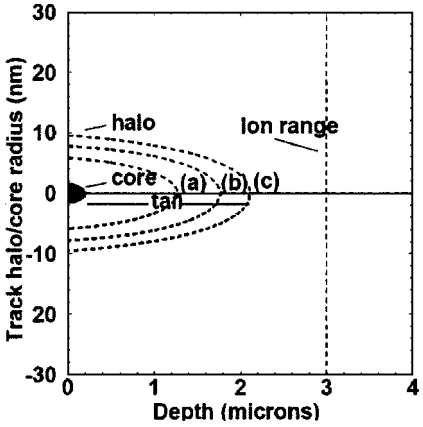

FIG. 1. Structure of the core, halo, and tail for 7.5-MeV Si ions on crystalline $LiNbO_3$. The ratio c_h/c_m is taken to be 10^{-1} (a), 10^{-2} (b), and 10^{-3} (c). The parameter values used are $kT_m/\varepsilon=0.20$, $S_m=4.75$ keV/nm, and $a_0=5.5$ nm. The value of S_m has been chosen for the purpose of illustrating the appearance of the track core.

$$L_t = z(S_h) - z(S_m), \tag{9}$$

where $z(S)$ is obtained by inverting the electronic stopping power function $S_e(z)$. As observed in Fig. 1 the length of the tail for $LiNbO_3$ irradiated with a silicon beam at 7.5 MeV is much larger than that of the latent track.

IV. FLUENCE DEPENDENCE OF THE AMORPHIZATION THRESHOLD: MEMORY EFFECT

A. Experimental results

High-energy silicon irradiation experiments at random incidence were performed at 5 and 7.5 MeV on congruent $LiNbO_3$ samples in the 5-MV tandetron accelerator recently installed[38] at the Centro de Microanálisis de Materials (Universidad Autónoma de Madrid). The samples were *Y*- and *Z*-cut plates of integrated optics quality purchased from Photox Optical Systems, U.K. The near-surface damage was monitored by measuring the refractive index profile with the dark *m*-lines technique. For comparison Rutherford backscattering spectroscopy (RBS) channeling data using H and He at 3 MeV were also taken along the *c* axial channel. The data are described in detail elsewhere.[32] Main relevant results from this study as well as from a recent work[31,33] using O, N, and F ions are as follows:

(a) For input energies such that the electronic stopping power at the surface S_e is close or above a threshold value $S_{e,\mathrm{th}}$, a homogeneous optically isotropic ("amorphous") surface layer is generated for fluences $\geqslant 10^{13}$ cm^{-2}. They present an abrupt refractive index profile as inferred from the resonances (unbound solutions of the wave equation) observed through the dark-mode *m*-lines technique (Fig. 2). The refractive index of the layer is $n=2.10$ which coincides with that reported[39] for amorphous $LiNbO_3$.

(b) The fluence necessary to initiate the surface layer depends critically on the value of the electronic stopping at the surface. For $S_e > S_m$ the layer starts just after overlapping of the individual latent tracks. For $S_e < S_m$ a certain fluence is required to start the amorphization process that increases with the difference $S_m - S_e$. Moreover, on increasing fluence the thickness h of the layer increases, as shown in Fig. 3(a). For equal fluences the thickness layer is thicker for the silicon beam at 7.5 MeV in comparison to 5 MeV as expected from the higher electronic stopping power. However, when the depth is scaled to the stopping power using the results of SRIM 2003 calculations the data for the two energies closely lie on the same curve, as illustrated in Fig. 3(b).

(c) RBS/channeling data using H and He ions at 3 MeV reveal that damage is cumulative until the homogeneous random (amorphous) layer is generated. This is

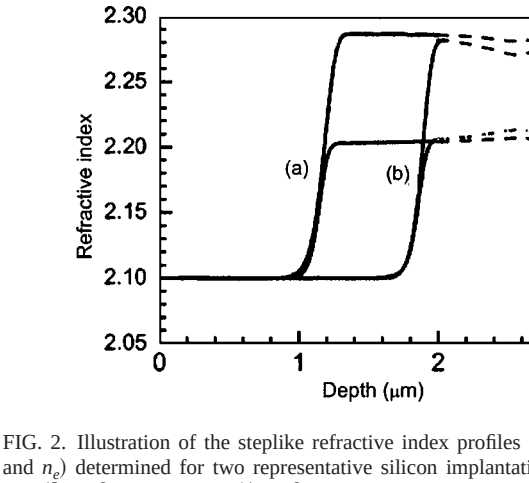

FIG. 2. Illustration of the steplike refractive index profiles (solid lines, n_o and n_e) determined for two representative silicon implantation fluences: 5×10^{13} cm^{-2} (a) and 3×10^{14} cm^{-2} (b) at 7.5 MeV. The dashed lines correspond to the estimated buried profiles due to the nuclear stopping power.

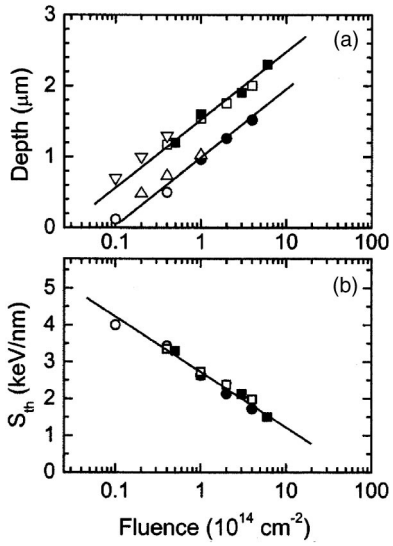

FIG. 3. Fluence dependence of the depth of the amorphous layer (a) and the corresponding modified electronic stopping power threshold S_{th} (b). The square symbols correspond to data from $LiNbO_3$ samples irradiated with 7.5-MeV silicon and to optical measurements (the closed symbols for *Y* cut and open symbols for *Z* cut). The closed circles correspond to data from $LiNbO_3$ samples irradiated with 5-MeV silicon and to optical measurements. The open circles correspond to the data obtained from RBS/channeling performed with He at 3 MeV [i.e., curves (c) and (d) in Fig. 4]. The open triangles correspond to complementary data obtained from RBS/channeling performed with H at 3 MeV on *Z*-cut $LiNbO_3$ irradiated with silicon at 5 MeV (upright triangles) and 7.5 MeV (inverted triangles).

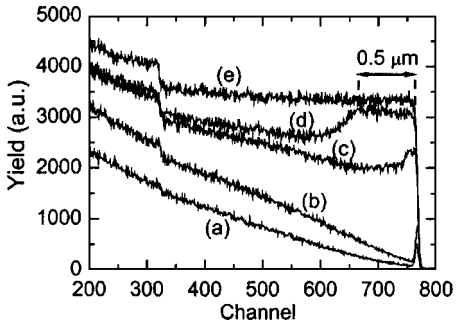

FIG. 4. Channeling RBS (with He at 3 MeV) spectra obtained along the *c* axis from *Z*-cut $LiNbO_3$ samples previously irradiated with 5-MeV silicon ions at fluences of 2×10^{12} at./cm^2 (b), 1×10^{13} at./cm^2 (c), and 4×10^{13} at./cm^2 (d). Curve (a) is the aligned spectrum in the virgin crystal and curve (e) the random spectrum.

clearly illustrated by the data taken with He for several irradiation fluences and displayed in Fig. 4.

These data cannot be explained by nuclear collision damage since no correlation is found with the nuclear stopping curve that peaks well inside the crystal and not at the surface. On the other hand, the existence of a threshold and the good correlation of the thickness of the amorphous layer (for different input energies) with the electronic stopping power [Fig. 3(b)] clearly supports an electronic excitation mechanism. Our basic assumption is that latent tracks are generated by electron excitation damage. After the fluence has reached a critical value to assure track overlapping a homogeneous amorphous layer is observed. By extrapolating the curve in Fig. 3(a) to zero thickness one finds a threshold value around or slightly above 5 keV/nm, consistent with those reported in the literature. In fact, reported data[23,24] for $LiNbO_3$ are in the range of 3–6 keV/nm.

The increase in thickness of the layer on going to higher fluences [Fig. 3] is not consistent with a fluence-independent threshold and clearly suggests that the threshold decreases with increasing fluence (*memory effect*). This effect implies a *synergy* between successive irradiations associated to either nuclear or electronic damage. The model we propose is that irradiation introduces some substantial electronic damage below the threshold value for amorphization (preamorphization stage). How to describe this stage and its effect on the threshold are the key points to be addressed in the paper.

B. Theoretical analysis: Surface amorphization

The preamorphized areas, particularly the tail, play an important role in the subsequent stages of damage, i.e., on the memory effect. This situation is well accepted for nuclear damage that is assumed to be permanent or accumulative (at low-enough temperatures). However, the situation has not been addressed for the case of the electronic damage, in spite of the extensive effort devoted to investigating the physical basis and finding technological applications for latent tracks. Let us consider an ion beam with energy E having an electronic stopping power S_e at a given depth z in the crystal. In this section we will refer, as a particular case, to $z=0$, i.e., to the input surface of the crystal. In the case of $S_e<S_m$, the maximum local concentration of defects generated is $c<c_m$. Therefore, latent tracks are not produced since electronic energy losses are below threshold. However, during irradiation intrinsic lattice defects will be introduced, facilitating the eventual achievement of threshold conditions for the next ions moving through the damaged areas.

After a fluence ϕ an average defect concentration $\overline{c}(\phi,S_e)$ has been produced. If $\overline{c}\geqslant c_m$ the crystal is already amorphized. Let us consider the case of $\overline{c}<c_m$. The additional defect concentration that another test particle must introduce in order to reach the threshold value for amorphization c_m is then $c=c_m-\overline{c}(\phi,S_e)$. From (6), the temperature that should be reached to generate that *additional* defect concentration, and so to melting of the previously damaged crystal is

$$T_{\max,\mathrm{th}}=\frac{\varepsilon/k}{\log_e A-\log_e \overline{c}(\phi,S_e)}=\frac{T_m}{1-\dfrac{kT_m}{\varepsilon}\log_e\left(1-\dfrac{\overline{c}}{c_m}\right)}. \quad (10)$$

The required increase in temperature over that of the substrate is then

$$T_{\max,\mathrm{th}}-T_s=\Delta T_{\mathrm{th}}=\frac{\Delta T_m}{1-\dfrac{kT_m}{\varepsilon}\log_e\left(1-\dfrac{\overline{c}}{c_m}\right)}\times\left[1+\frac{T_s}{\Delta T_m}\frac{kT_m}{\varepsilon}\log_e\left(1-\frac{\overline{c}}{c_m}\right)\right], \quad (11)$$

with $\Delta T_m=T_m-T_s$. The threshold value of S_e that leads to this increase in temperature can then be obtained by replacing in (3) and will be designated as S_{th}. It represents the threshold for amorphization after the crystal has received an irradiation fluence ϕ. One arrives at

$$S_{\mathrm{th}}(\phi,S_e)=\frac{S_m}{1-\dfrac{kT_m}{\varepsilon}\log\left[1-\dfrac{\overline{c}(\phi,S_e)}{c_m}\right]}\times\left\{1+\frac{T_s}{\Delta T_m}\frac{kT_m}{\varepsilon}\log_e\left[1-\frac{\overline{c}(\phi,S_e)}{c_m}\right]\right\},\quad \overline{c}(\phi,S_e)<c_m. \quad (12)$$

Note that in the absence of any previous irradiation $\overline{c}=0$ and $S_{\mathrm{th}}(0,S_e)=S_m$. The function $\overline{c}(\phi,S_e)$ can be readily calculated as

$$\overline{c}(\phi,S_e)=N\int\int_A c[T_{\max}(r,S_e)]\frac{dxdy}{A}, \quad (13)$$

where x and y are the Cartesian coordinates at the surface, A the area of the irradiated region, and N the total number of incident particles. Noticing that the fluence is just $\phi=N/A$ and that the integrand is nonzero in a very small region as compared to the macroscopic domain A, the limits of the integral can be extended to infinity. Transforming to polar coordinates one obtains

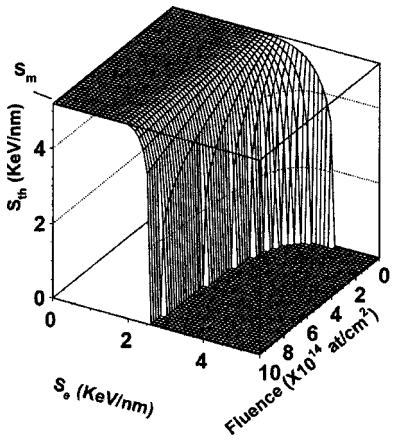

FIG. 5. Electronic stopping power threshold for amorphization (S_{th}) as a function of prior irradiation with a fluence of ions having an electronic stopping power S_e. The parameter values used are $kT_m/\varepsilon=0.20$, $S_m=5.2$ keV/nm, and $a_0=5.5$ nm.

$$\overline{c}(\phi,S_e)=2\pi\phi\int_0^\infty rc[T_{\max}(r,S_e)]dr. \tag{14}$$

This integral uses expressions (2) and (6). It has to be divided into two summands, according to the piecewise definition of $\Delta T(r,S_e)$. The result of the calculation, that requires some algebra is

$$\frac{\overline{c}(\phi,S_e)}{c_m}=2\pi\phi a_0^2\left\{\int_1^e\frac{1}{u}\exp\left[-\frac{\varepsilon}{kT_m}\left(\frac{S_m}{S_e}t-1\right)\right]du+\frac{1}{e}\frac{kT_m}{\varepsilon}\frac{S_e}{S_m}\exp\left[-\frac{\varepsilon}{kT_m}\left(\frac{S_m}{S_e}e-1\right)\right]\right\}. \tag{15}$$

This result can be readily replaced in (12) to yield the modified threshold for lattice amorphization after an irradiation of fluence ϕ with ions having a stopping power S_e in a material having a threshold S_m prior to irradiation. Note that the critical concentrations c_m and c_h do not explicitly appear in (12) after inserting the result of (15). In fact, the only relevant parameters of the theory are ε and a_0 (aside from S_m).

The theoretical dependence $S_{th}(\phi,S_e)$, obtained by numerical calculation of expressions (12) and (15), has been plotted in Fig. 5 for the following reasonable set of parameters: $kT_m/\varepsilon=0.2$, $S_m=5.2$ keV/nm, and $a_0=5.5$ nm. The value for the thermal activation energy represents the best choice to fit all the experimental data described in this paper as well as those recently reported.[33] The threshold lies within the range reported from single track experiments.[23,24] The value for a_0 gives the best fitting to our data and it is close to the value of 4.5 obtained for a variety of insulator crystals.[16] $S_{th}(\phi,S_e)$ constitutes a *universal* or *reference* surface in the sense that it applies to any bombarding ion and energy on $LiNbO_3$.

In Fig. 6 we show the fluence necessary to start amorphization at the surface, as a function of Se. It has been obtained from Fig. 5 after the cutting of the reference surface by the bisector plane $S_{th}=S_e$. The theoretical curve has been compared to experimental data[33] on N (4.53 MeV), O (5.00 MeV), and F (5.13 MeV), and to those presented in this work for Si (5 MeV). The data very well fit the model predictions for the selected set of parameters.

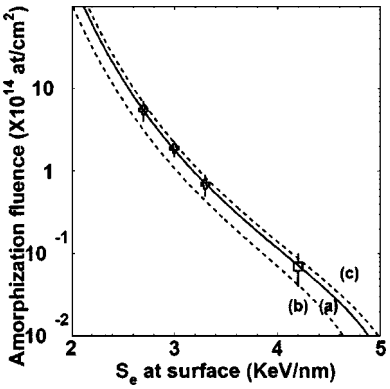

FIG. 6. Theoretical prediction of the fluence necessary to start amorphization at the surface of a $LiNbO_3$ crystal as a function of the electronic stopping power of the bombarding ions. The parameter values used are $kT_m/\varepsilon=0.20$, $a_0=5.5$ nm, and $S_m=5.2$ keV/nm [curve (a)], 4.94 keV/nm (b), and 5.3 keV/nm (c). Experimental data taken from Ref. 33 (crosses) and from this work (squares) are given for comparison. S_m values [(b) and (c)] include a linear ion velocity-dependent correction [(b) for crosses and (c) for squares].

C. Theoretical analysis: Propagation of the amorphization front

A main consequence of the memory effect described in Sec. IV B is the propagation of the amorphous-crystalline boundary into the crystal during irradiation. The reason is that previous irradiation decreases the threshold at any depth z below the ion range. In order to describe how the amophization front propagates into the sample one just needs to add to formula (12), valid for all depths, the constraint $S_{th}(\phi,S_e)=S_e$. This is an implicit equation from which S_e can be obtained as a function of ϕ (i.e., the same procedure followed at the end of the previous section in order to analyze the behavior at the surface). Replacing S_e by the stopping power curve $S_e(z)$ of the bombarding ion derived from SRIM 2003 (Fig. 7), one finally obtains the relation among z, ϕ, and S_e, schematically written as

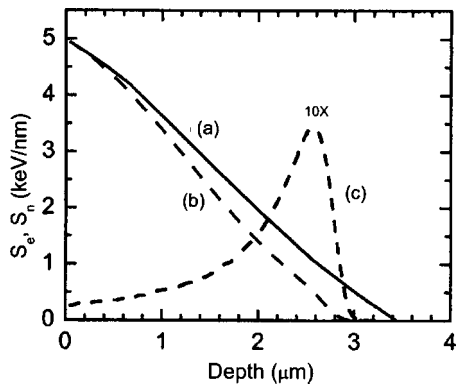

FIG. 7. Theoretical electronic [(a) and (b)] and nuclear (c) stopping power curves for silicon 7.5 MeV in $LiNbO_3$ calculated with SRIM 2003. Curves (b) and (c) correspond to the crystalline $LiNbO_3$ phase. Curve (a), used in the calculations of the model, is the corrected curve assuming an amorphous layer with a progressively increasing thickness and a 15% decrease of density.

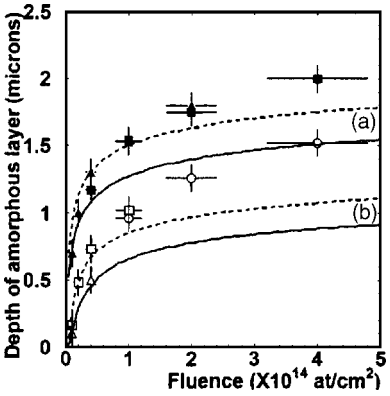

FIG. 8. Theoretical prediction of the depth z of the amorphization front as a function of 7.5-MeV (a) and 5-MeV (b) Si-ion fluences, compared to experimental data (this work). The parameter values used are $kT_m/\varepsilon=0.20$, $S_m=5.2$ keV/nm, and $a_0=5.5$ nm (solid curve). The dashed line shows the result of including a velocity-dependent correction to S_m, as explained in the text. The full symbols correspond to 7.5-MeV Si-ion data and the open symbols to 5-MeV Si. The circles stand for optical measurements, squares for H channeling, and triangles for He channeling.

$$S_{\mathrm{th}}[\phi, S_e(z)] = S_e(z). \tag{16}$$

In other words one is able to obtain the depth of the amorphization front after a fluence ϕ.

Although the problem is essentially similar to the one dealt with in Sec. IV, it is more complex. In fact, the ions arriving into the amorphous-crystalline boundary have moved through a previously amorphized (lower density) layer and so they undergo a lower stopping power than in crystalline $LiNbO_3$. Therefore, one has to use a corrected $S_e(z)$ curve (see Fig. 7) that takes into account the reduced stopping power of the amorphous layer on top of the considered z plane. The corrected function calculated also with the SRIM 2003 code for amorphous $LiNbO_3$ (density of 15% lower) and displayed in Fig. 7 has been introduced in (16) to find numerically the dependence $z(\phi)$. Figure 8 shows the numerical solutions for 7.5 and 5-MeV silicon irradiations on $LiNbO_3$ together with the set of data points of Fig. 4. The values selected for the parameters are the same as in Fig. 6. The prediction of the model with this chosen set of parameters is depicted as a solid line. It is clear that the main experimental trend is well accounted for by theory. There is an initial rapid propagation of z with ϕ, followed by a nearly saturating stage. The quantitative agreement is worse. The data points corresponding to the highest fluences appear at depths significantly larger than the predicted ones. However, from Fig. 7 one sees that the contribution of nuclear damage is very relevant at this large depth and it has not been taken into account in our analysis.

Within the purely electronic losses regime, there may be another contribution to the discrepancy between theory and experiment. It is well known that the threshold for latent track formation markedly decreases on decreasing ion velocity[24,40–42] (*velocity effect*). This effect has been investigated at various energies within a broad range going from 0.05 to 2 MeV/nucleon, in which range the threshold varies[23] from around 3 to around 6 keV/nm. It has been concluded that a substantial decrease in threshold (increase in the efficiency factor g) occurs when passing from the high-velocity to the low-velocity regime. This effect, that acts in the right direction to reduce the discrepancy between theory and experiment, has not been considered in our model and it is outside the scope of this paper. However, as an orientation of the trend that the calculation would take by including it, the fixed value $S_m=5.2$ has been replaced by a function linear on the ion velocity, such as $S_m=5.2$ keV/nm for Si at 7.5 MeV and $S_m=4.68$ keV/nm at 2.8 MeV. This implies a reduction of 10% in the threshold value on going from 0.27 to 0.1 MeV/amu. The result of this modification to the calculation is shown as the dashed curves in Fig. 8. Notice that the agreement between model and data is already much better even with this very naive implementation of the velocity dependence of the threshold. For the sake of consistency, the same velocity dependence has been included in Fig. 6.

V. SUMMARY AND FINAL COMMENTS

A simple model has been proposed to describe the damage along and around the trajectory of high-energy bombarding ions in insulating crystals. For electronic stopping powers above a threshold value the damage region includes a surrounding halo and a tail aside from the amorphous core (latent track). Estimates for the radius of the halo and the length of the tail have been given as a function of the input stopping power. The model predicts that previous irradiation reduces the latent track threshold at the surface and yields a simple analytical expression for the dependence of this threshold on prior fluence, *memory effect*. Experimental data using N (4.53 MeV), O (5.00 MeV), F (5.13 MeV), and Si (5 MeV) fit very well the theoretical curve. Moreover, the propagation of the amorphization front with fluence has been theoretically described. The results are in reasonable agreement with experiments using Si (5 and 7.5 MeV), that can be markedly improved when an *ad hoc* correction for the velocity effect on the threshold is considered. The agreement deteriorates for the largest fluences or depths, possibly due to the contribution of nuclear collision damage. In summary, the model is simple and versatile enough to provide useful predictions and guide experimental work.

[1] J. K. Hirvonen, *Ion Implantation and Ion Beam Processing* (North Holland, Amsterdam, 1984).
[2] F. Agulló-López, C. R. A. Catlow, and P. D. Townsend, *Point Defects in Materials* (Academic, London, 1988).
[3] J. F. Ziegler, *Ion Implantation Technology* (North Holland, Amsterdam, 1992).
[4] P. D. Townsend, P. J. Chandler, and L. Zhang, *Optical Effects of Ion Implantation* (Cambridge University Press, Cambridge, 1994).
[5] E. C. M. Silk and R. S. Barnes, Philos. Mag. **4**, 970 (1959).
[6] A. Sigrist and R. Balzer, Helv. Phys. Acta **50**, 49 (1977).
[7] R. L. Fleischer, P. B. Price, and R. M. Walker, *Nuclear Tracks in Solids* (University of California Press, Berkeley, 1975).
[8] M. Toulemonde, S. Bouffard, and F. Studer, Nucl. Instrum. Methods Phys. Res. B **91**, 108 (1994).
[9] R. Spohr, in *Ion Tracks and Microtechnology: Basic Principles and Applications*, edited by K. Bethge (Vieweg, Braunchsweig, 1990).
[10] E. Ferain and R. Legras, Nucl. Instrum. Methods Phys. Res. B **174**, 116 (2001).
[11] M. E. Toimil Morales, E. M. Hohberger, Ch. Schaeflein, R. H. Blick, R. Neumann, and C. Trautmann, Appl. Phys. Lett. **82**, 2139 (2003).
[12] L. Piraux, J. M. George, J. F. Despres, C. Leroy, E. Ferain, R. Legras, K. Ounajdela, and A. Fert, Appl. Phys. Lett. **65**, 2484 (1994).

[13]M. S. Gudiksen, J. Wang, and C. M. Lieber, J. Phys. Chem. B **106**, 4036 (2002).
[14]M. Toulemonde, C. Trautmann, E. Balanzat, K. Hjort, and A. Weidinger, Nucl. Instrum. Methods Phys. Res. B **216**, 1 (2004).
[15]M. I. Kaganov, I. M. Lifshitz, and L. V. Tanatarov, Sov. Phys. JETP **4**, 173 (1957).
[16]G. Szenes, Mater. Sci. Forum **97–99**, 647 (1992); Nucl. Instrum. Methods Phys. Res. B **122**, 530 (1997).
[17]M. Toulemonde, C. Dufour, and E. Paumier, Phys. Rev. B **46**, 14362 (1992).
[18]M. Toulemonde, C. Dufour, and E. Paumier, Radiat. Eff. Defects Solids **126**, 201 (1993).
[19]G. Szenes, Phys. Rev. B **51**, 8026 (1995).
[20]Z. G. Wang, Ch. Dufour, E. Paumier, and M. Toulemonde, J. Phys.: Condens. Matter **6**, 6733 (1994); **7**, 2525 (1995); Nucl. Instrum. Methods Phys. Res. B **115**, 577 (1996).
[21]M. Toulemonde, J. M. Constantini, Ch. Dufour, A. Meftah, E. Paumier, and F. Studer, Nucl. Instrum. Methods Phys. Res. B **116**, 37 (1996).
[22]M. Toulemonde, Ch. Dufour, Z. G. Wang, and E. Paumier, Nucl. Instrum. Methods Phys. Res. B **112**, 26 (1996).
[23]B. Canut and S. M. M. Ramos, Radiat. Eff. Defects Solids **145**, 1 (1998).
[24]M. Toulemonde, Ch. Dufour, A. Meftah, and E. Paumier, Nucl. Instrum. Methods Phys. Res. B **166–167**, 903 (2000).
[25]R. Kelly and A. Miotello, Nucl. Instrum. Methods Phys. Res. B **141**, 49 (1998).
[26]M. Beuve, N. Stolterfoht, M. Toulemonde, C. Trautman, and H. M. Urbassek, Phys. Rev. B **68**, 125423 (2003).
[27]C. Trautmann, M. Boccanfuso, A. Benyagoub, S. Klaumunzer, K. Schwartz, and M. Toulemonde, Nucl. Instrum. Methods Phys. Res. B **191**, 144 (2002).
[28]E. M. Bringa and R. E. Johnson, Nucl. Instrum. Methods Phys. Res. B **143**, 513 (1998).
[29]E. M. Bringa, R. E. Johnson, and M. Jakas, Phys. Rev. B **60**, 15107 (1999).
[30]M. M. Jakas, E. M. Bringa, and R. E. Johnson, Phys. Rev. B **65**, 165425 (2002).
[31]G. G. Bentini *et al.*, J. Appl. Phys. **92**, 6477 (2002).
[32]J. Olivares, G. García, F. Agulló-López, F. Agulló-Rueda, A. Kling, and J. C. Soares, Appl. Phys. A: Mater. Sci. Process. (in press).
[33]G. G. Bentini *et al.*, J. Appl. Phys. **96**, 242 (2004).
[34]*Properties of Lithium Niobate*, EMIS Datareview Series, edited by K. K. Wong (INSPEC, Exeter, 2002).
[35]T. van Dillen, A. Polman, W. Fukarek, and A. van Blaaderen, Appl. Phys. Lett. **78**, 910 (2001).
[36]J. Frantz, J. Tarus, K. Nordlund, and J. Keinonen, Phys. Rev. B **64**, 125313 (2001).
[37]J. Frenkel, *Kinetic Theory of Liquids* (Dover, New York, 1955).
[38]D. J. W. Mous, A. Gottdang, R. G. Haitsma, G. García López, A. Climent-Font, F. Agulló-López, and D. O. Boerma, in *Application of Accelerators in Research and Industry*, edited by Jerome L. Duggan, AIP Conf. Proc. No. 680 (AIP, Melville, NY, 2003), p. 999.
[39]G. L. Destefanis, G. P. Gaillard, L. Ligeon, S. Valette, B. W. Farmery, P. D. Townsend, and A. Perez, J. Appl. Phys. **50**, 7898 (1980).
[40]G. Szenes, Nucl. Instrum. Methods Phys. Res. B **191**, 54 (2002).
[41]G. Szenes, F. Pászti, A. Péter, and D. Fink, Nucl. Instrum. Methods Phys. Res. B **191**, 186 (2002).
[42]A. Meftah, F. Brisard, J. M. Constantini, M. Hage-Ali, J. P. Stoquert, F. Studer, and M. Toulemonde, Phys. Rev. B **48**, 920 (1993).